Biomaterials 274 (2021) 120876

Contents lists available at ScienceDirect

Biomaterials

journal homepage: www.elsevier.com/locate/biomaterials

Digital CRISPR-based method for the rapid detection and absolute quantification of nucleic acids

Xiaolin Wu [a], Joshua K. Tay [b], Chuan Keng Goh [b], Cheryl Chan [a], Yie Hou Lee [a], Stacy L. Springs [a,c], De Yun Wang [b], Kwok Seng Loh [b], Timothy K. Lu [a,d,e,f,g,h,i,**], Hanry Yu [a,j,k,l,*]

[a] Critical Analytics for Manufacturing Personalized Medicine Interdisciplinary Research Group, Singapore-MIT Alliance for Research and Technology, 138602, Singapore
[b] Department of Otolaryngology-Head and Neck Surgery, National University of Singapore, Singapore
[c] Center for Biomedical Innovation, Massachusetts Institute of Technology, Cambridge, MA, 02139, USA
[d] Synthetic Biology Center, Massachusetts Institute of Technology (MIT), Cambridge, MA, 02139, USA
[e] Synthetic Biology Group, Research Laboratory of Electronics, Massachusetts Institute of Technology (MIT), Cambridge, MA, 02139, USA
[f] Broad Institute of MIT and Harvard, Cambridge, MA, 02142, USA
[g] Department of Electrical Engineering and Computer Science, Massachusetts Institute of Technology (MIT), Cambridge, MA, 02142, USA
[h] Harvard-MIT Division of Health Sciences and Technology, Cambridge, MA, 02139, USA
[i] Department of Biological Engineering, Massachusetts Institute of Technology (MIT), Cambridge, MA, 02142, USA
[j] Institute of Bioengineering and Bioimaging, A*STAR, The Nanos, #04-01, 31, Biopolis Way, 138669, Singapore
[k] Mechanobiology Institute, National University of Singapore, T-Lab, #05-01, 5A Engineering Drive 1, 117411, Singapore
[l] Department of Physiology & the Institute for Digital Medicine (WisDM), Yong Loo Lin School of Medicine, MD9-04-11, 2 Medical Drive, 117593, Singapore

ARTICLE INFO

Keywords:
CRISPR/Cas
Absolute quantification
Molecular diagnosis
Virus detection

ABSTRACT

Rapid diagnostics of adventitious agents in biopharmaceutical/cell manufacturing release testing and the fight against viral infection have become critical. Quantitative real-time PCR and CRISPR-based methods rapidly detect DNA/RNA in 1 h but suffer from inter-site variability. Absolute quantification of DNA/RNA by methods such as digital PCR reduce this variability but are currently too slow for wider application. Here, we report a RApid DIgital Crispr Approach (RADICA) for absolute quantification of nucleic acids in 40-60 min. Using SARS-CoV-2 as a proof-of-concept target, RADICA allows for absolute quantification with a linear dynamic range of 0.6–2027 copies/μL (R^2 value > 0.99), high accuracy and low variability, no cross-reactivity to similar targets, and high tolerance to human background DNA. RADICA's versatility is validated against other targets such as Epstein-Barr virus (EBV) from human B cells and patients' serum. RADICA can accurately detect and absolutely quantify EBV DNA with similar dynamic range of 0.5–2100 copies/μL (R^2 value > 0.98) in 1 h without thermal cycling, providing a 4-fold faster alternative to digital PCR-based detection. RADICA therefore enables rapid and sensitive absolute quantification of nucleic acids which can be widely applied across clinical, research, and biomanufacturing areas.

1. Introduction

Methods to rapidly detect and absolutely quantify adventitious agents such as viruses are needed to monitor and halt the spread of infectious diseases, to accelerate the virus-related research, and critical in biosafety release testing in biopharmaceutical and cell manufacturing process [1–3]. Regulatory guidelines from the United States Food and Drug Administration (FDA) often mandate the identification of live adventitious agents, i.e. their replication competency [4] that can benefit from the rapid diagnostic methods that allow their absolute quantification. Reverse transcription-quantitative polymerase chain reaction (RT-qPCR) is considered a gold standard for viral detection [5].

* Corresponding author. Critical Analytics for Manufacturing Personalized Medicine Interdisciplinary Research Group, Singapore-MIT Alliance for Research and Technology, 138602, Singapore.
** Corresponding author. Critical Analytics for Manufacturing Personalized Medicine Interdisciplinary Research Group, Singapore-MIT Alliance for Research and Technology, 138602, Singapore.
E-mail addresses: timlu@mit.edu (T.K. Lu), phsyuh@nus.edu.sg (H. Yu).

https://doi.org/10.1016/j.biomaterials.2021.120876
Received 1 December 2020; Received in revised form 23 April 2021; Accepted 2 May 2021
Available online 11 May 2021

However, quantification by RT-qPCR relies on the use of accurate and stable external standards or references, with a 20–30% variability reported even within trained laboratories or testing sites [2,6,7]. Thus, an absolute quantification method with improved speed is needed for establishing reference benchmarks, and for allowing reliable cross-site standardized comparisons in international research collaborations, global health surveillance, and food and drug safety supervision/surveillance [8,9]. We hypothesize that a rapid, sensitive and specific diagnostics method capable of absolute quantification of viral nucleic acids can be developed by integrating the CRISPR-based isothermal amplification and digital PCR (dPCR)-based partitioning approaches.

dPCR is increasingly being used as a highly accurate and sensitive method for absolute quantification of nucleic acids [2,8,10,11]. Since thousands of PCR reactions take place in individual partitions independently, absolute quantification by dPCR is more robust than RT-qPCR, less sensitive to inhibitors and poor amplification efficiency [2,7]. dPCR-based viral detection can quantitatively detect SARS-CoV-2 in the COVID-19 patient samples with reduced inter-site variability, with fewer false negatives and false positives than using RT-qPCR [12–14]. dPCR has also been applied to study the aerodynamic transmission of SARS-CoV-2 [15]. The main drawback of dPCR; however, is the relatively long reaction time (~4 h), which hinders wider applications [8].

Isothermal amplification is a faster approach to amplify the target nucleic acids at a constant temperature, thereby reducing reaction time, and may employ recombinase polymerase amplification (RPA) or loop-mediated isothermal amplification (LAMP) [16,17]. To reduce the nonspecific amplification of RPA or LAMP, RNA-guided CRISPR/Cas system were used to tag the specific sequence of the target DNA/RNA. In the RNA-guided CRISPR/Cas system, Cas12a and Cas13a effectors are exploited for their collateral cleavage activity, i.e., the degradation of nonspecific fluorescently-tagged reporter oligos (FQ reporter), once the Cas protein finds and cleaves a specific DNA/RNA target [18,19]. By combining RPA- or LAMP-mediated isothermal amplification of target molecules with CRISPR/Cas biosensing, researchers have developed SHERLOCK, HOLMES and DETECTR to detect dengue virus and human papillomavirus, as well as SARS-CoV-2 [20–28]. However, the non-quantitative nature and complex multiple operations of CRISPR-based methods prevent their widespread use. After we have reported this work in MedRxiv, three digital CRISPR-based methods were reported to detect SARS-CoV-2 [29–31], two without demonstrating absolute quantification and one is limited to RNA detection.

We report here a RApid DIgital Crispr Approach (RADICA) that offers absolute quantification of nucleic acids in 40-60 min, which is four times faster than dPCR. This method combines the advantages of quantitative dPCR, rapid isothermal amplification, and specific CRISPR/Cas-based detection into a one-pot reaction system that partitions individual reactions into ten thousand compartments on a high-density chip. We validated this method using DNA containing the N (nucleoprotein) gene of SARS-CoV-2 and showed a linear signal-to-input response of R^2 value > 0.99, with comparative sensitivity and accuracy to dPCR. The method is highly specific to the target nucleic acids, without cross-reactivity to other similar targets, and is insensitive to human background DNA. The broad applicability of RADICA was demonstrated in the absolute quantification of Epstein-Barr virus from virus-infected human B cells (R^2 value > 0.98) and validated in monitoring the EBV cell-free DNA in 145 human serum. RADICA is a rapid and sensitive diagnostics method for the accurate detection and absolute quantification of nucleic acids in 40-60 min, with potential for wide applications.

2. Materials and methods

2.1. Materials

Preparation of primers and DNA targets: Oligonucleotides (primers), ssDNA-FQ reporters, SARS-CoV-2 N gene-containing G-Block dsDNA, SARS-CoV-2, SARS-CoV, and MERS N gene-containing plasmids were synthesized by or purchased from Integrated DNA Technologies. The sequences related to this study are listed in Supplementary Table 1. The SARS-CoV-2 N gene-containing plasmid (IDT) was linearized using FastDigest ScaI (Thermo Scientific) and then used as DNA targets. The SARS-CoV-2 N gene-containing plasmid was used as a template to amplify the N gene using primer N-RNA-F/N-RNA-R by Platinum™ SuperFi II PCR Master Mix (Invitrogen). The PCR product was purified by QIAquick PCR Purification Kit (QIAGEN) and used as RNA synthesis templates.

Synthetic RNA target: Since N-RNA-F has a T7 promoter sequence, the amplified DNA using N-RNA-F/R primer will contain a T7 promoter upstream of gene N. The T7 tagged N gene dsDNA was transcribed into SARS-CoV-2 RNA using HiScribe™ T7 High Yield RNA Synthesis Kit (New England Biolabs) according to the manufacturer's protocol. The synthesized RNA (N gene) was purified using the Monarch® RNA Cleanup Kit (New England Biolabs) after treatment with DNase I (RNase-free, New England Biolabs). The synthetic RNA covering 99.9% of the bases of the SARS-CoV-2 viral genome were purchased from Twist Bioscience (Genbank ID: MN908947.3).

crRNA preparation: Constructs were ordered as DNA from Integrated DNA Technologies with an appended T7 promoter sequence. crRNA ssDNA was annealed to a short T7 primer (T7-3G IVT primer [32] or T7-Cas12scaffold-F [33]) and treated with fill-in PCR (Platinum™ SuperFi II PCR Master Mix) to generate the DNA templates. These DNA were used as templates to synthesize crRNA using the HiScribe™ T7 High Yield RNA Synthesis Kit (New England Biolabs) according to published protocols [32,33]. The synthesized crRNA was purified using the Monarch® RNA Cleanup Kit (New England Biolabs) after treatment with DNase I (RNase-free, New England Biolabs), Thermolabile Exonuclease I (New England Biolabs), and T5 Exonuclease (New England Biolabs).

2.2. Primer and crRNA design

SARS-CoV-2 primers and crRNA were designed based on previously published papers [26] or 264 SARS-CoV-2 genome sequences from GISAID [34,35]. Other human-related coronavirus sequences were downloaded from NCBI. UGENE software was used to analyze and align viral genomes (MUSCLE or Kalign). Consensus sequences (threshold: 90%) of 264 SARS-CoV-2 genomes, 328 SARS-CoV, 572 MERS-CoV, 70 Human-CoV-229E genomes, 48 Human-CoV-HKU1 genomes, 71 Human-CoV-NL63, and 178 Human-CoV-OC43 were exported separately from UGENE and used for specificity analysis.

Epstein-Barr virus primers and crRNA were designed based on consensus sequences of 16 virus genomes, including both type I and type II EBV (NCBI: AP015016.1, AY961628.3, HQ020558.1, JQ009376.2, KC207813.1, KC207814.1, KC440851.1, KC440852.1, KC617875.1, KF373730.1, KF717093.1, KP735248.1, LN827800.1, NC_007605.1, NC_009334.1, V01555.2).

2.3. Digital PCR quantification

SARS-CoV-2 N gene quantification: The G-block dsDNA, plasmid, dsDNA and RNA concentrations were quantified by dPCR. Serial dilutions of targets were mixed with 500 nM CHNCDC-geneN-F, 500 nM CHNCDC-geneN-R, 250 nM CHNCDC-geneN-P, 1x TaqMan™ Fast Virus 1-Step Master Mix (for RNA, Applied Biosystems) or TaqMan™ Fast Advanced Master Mix (for DNA, Applied Biosystems), 1x Clarity™ JN solution (JN Medsys). For RNA samples, the reaction mixture was incubated at 55 °C 5 min before partitioning the reaction mix on Clarity™ autoloader. Then the reaction partitions were sealed with the Clarity™ Sealing Enhancer and 230 μL Clarity™ Sealing Fluid, followed by thermal cycling using the following parameters (ramp rate = 1 °C/s): 95 °C for 15 min (one cycle), 95 °C 50 s and 56 °C 90 s (40 cycles), 70 °C

5 min (one cycle). The endpoint fluorescence of the partitions was detected using Clarity™ Reader and the final DNA copy numbers were analyzed by Clarity™ software.

EBV quantification: Serial dilutions of EBV DNA were used for dPCR quantification by Clarity™ Epstein-Barr Virus Quantification Kit (JN Medsys) or primers and probes from published papers [36,37] with TaqMan™ Fast Advanced Master Mix (Applied Biosystems), 1x Clarity™ JN solution (JN Medsys) according to the manufacturer's protocol.

2.4. Cas12a bulk assay without preamplification

Unless otherwise indicated, 50 nM EnGen® Lba Cas12a (New England Biolabs), 50 nM crRNA, and 250 nM FQ reporter were incubated with dsDNA dilution series in NEB buffer 2.1 at 37 °C, and fluorescence signals were measured every 5 min.

2.5. RPA-Cas12a bulk assay

The one-pot reaction combining RPA-DNA amplification and Cas12a detection was performed as follows: 300 nM forward primer, 300 nM reverse primer, 500 nM FQ reporter, 1x RPA rehydration buffer containing 1 x RPA Pellet (TwistDx), 200 nM EnGen® Lba Cas12a (New England Biolabs), 200 nM crRNA, were prepared followed by adding various amounts of DNA input, and 14 mM magnesium acetate. When RNA was used as a target, 300 nM reverse primer 2 was used with 10 U/μL PhotoScript Reverse transcriptase (New England Biolabs) or 10 U/μL SuperScript™ IV Reverse Transcriptase (Invitrogen) and 0.5 U/μL RNase H (Invitrogen or New England Biolabs), as indicated. When detecting RPA signal is needed, 250 mM SYTO-82 fluorescent nucleic acids stain was added into the reaction. The reaction mixture was incubated at 42 °C unless otherwise indicated and fluorescence kinetics were monitored every 1 min.

2.6. RADICA quantification

Commercial chips for sample partitioning and matched fluorescence reader for endpoint detection were used in RADICA [38]. The RADICA reaction was prepared by adding 1x Clarity™ JN solution (JN Medsys) to the RPA-Cas12a bulk reactions stated above. To prevent spontaneous target amplification by RPA at room temperature [39], the RPA-CRISPR reaction was prepared without the addition of Mg^{2+}, which is required for the polymerase activity. All reactions were prepared on ice and samples were loaded within 1 min after adding Mg^{2+} to prevent premature target amplification. 15 μL of the mixture was loaded on the chip by a Clarity™ autoloader for sample partitioning. The reaction partitions were sealed with the Clarity™ Sealing Enhancer and 230 μL Clarity™ Sealing Fluid. The partitioned reactions were incubated in water baths or heat blocks at 42 °C for 1 h, unless otherwise indicated. After incubation, a Clarity™ Reader was used to read the fluorescent signal in the partitions, and Clarity™ software was used to calculate input DNA copy numbers.

2.7. Limit of blank (LoB), lower limit of detection (LLoD), and lower limit of quantitation (LLoQ) calculation

LoB, LLoD, and LLoQ were calculated based on the following equation [40] using the statistics of RADICA quantification on linearized plasmids in 10 replications (Supplementary Table 2):

$\text{LoB} = \text{mean}_{\text{blank}} + 1.645\ (\text{SD}_{\text{blank}})$.

$\text{LLoD} = \text{LoB} + 1.645\ (\text{SD}_{\text{low concentration sample}})$.

LLoQ = the lowest concentration of CV $\leq$ 15%

2.8. Growing EBV-2 from Jijoye cells

Jijoye cells were treated with 4 mM sodium butyrate and 24 ng/mL tetradecanoyl phorbol acetate (TPA). Supernatants were harvested 4–5 days post-treatment by centrifugation at 4,000 x g for 20 min and passing over a 0.45 μm filter to remove cellular debris. Viral particles were pelleted by ultracentrifugation at 20,000 rpm for 90 min and resuspended in 1/100 the initial volume using complete RPMI or PBS if viruses were to be further purified. Concentrated viruses were further purified using OptiPrep gradient density ultracentrifugation at 20,000 rpm for 120 min, and the virus interface band was collected and stored at −80 °C for downstream analysis.

2.9. Epstein-Barr virus DNA extraction from Jijoye cells

EBV DNA was extracted using the QIAamp DNA Mini Kit (QIAGEN) according to the manufacturer's protocol.

2.10. Clinical samples for Epstein-Barr virus detection

Two sets of clinical samples from a serum bank of nasopharyngeal cancer patients and healthy controls were used in this study [37,41]. The first set comprised 79 serum samples of which 39 were from nasopharyngeal cancer (NPC) patients and 40 were from healthy controls. The second set comprised of 66 serum samples taken from 22 NPC patients at three time points: at the time of initial diagnosis, one year after treatment and at the time of recurrence. All participants were recruited with informed consent, and the study was approved by the Institutional Review Board of the National Healthcare Group, Singapore (Approval numbers: 2006/00149, 2006/00409).

2.11. Epstein-Barr virus DNA extraction from serum

EBV cell-free DNA was extracted from 200 μL of serum using the ReliaPrep™ Blood gDNA Miniprep System (Promega) according to the manufacturer's protocol. The DNA was eluted using 50 μL of ddH_2O and further diluted using another 50 μL of ddH_2O, resulting in 100 μL of DNA solution.

2.12. qPCR quantification of Epstein-Barr virus in serum cell-free DNA

qPCR was performed using 400 nM EBNA-PCR-F, 400 nM EBNA-PCR-R, 200 nM EBNA-P-FAM, 200 nM BamHIW-PCR-44F, 200 nM BamHIW-PCR-119R, 100 nM BamHIW-P-HEX, 3 μL of serum DNA (after 1:1 dilution) or controls in 1x TaqMan™ Fast Advanced Master Mix (Applied Biosystems). Each reaction mix was incubated at 50 °C 2min to allow UNG to degrade carry-over PCR products, followed by 1 cycle at 95 °C for 2 min, 45 cycles at 95 °C for 3 s and 59 °C for 30 s. A standard curve using DNA extracted from the Jijoye EBV positive cell line was run in parallel with each reaction to quantify the input DNA concentration.

2.13. dPCR quantification of Epstein-Barr virus in serum cell-free DNA

dPCR was performed using the Clarity Digital PCR System (JN Medsys). Each 15 μL dPCR reaction consisted of 400 nM EBNA-PCR-F, 400 nM EBNA-PCR-R, 200 nM EBNA-P-FAM, 200 nM BamHIW-PCR-44F, 200 nM BamHIW-PCR-119R, 100 nM BamHIW-P-HEX, 1x Clarity JN Solution (JN Medsys), 1x TaqMan™ Fast Advanced Master Mix (Applied Biosystems), and 3 μL of serum DNA or controls. Each reaction mix was partitioned in the Clarity Digital PCR tube-strip (JN Medsys) followed by 1 cycle at 95 °C for 10 min, 40 cycles at 95 °C for 50 s and 57 °C for 90 s and 1 cycle at 70 °C for 5 min (ramp rate = 1 °C/s). After thermal cycling, a Clarity™ Reader was used to read the fluorescent signal in the partitions, and Clarity™ software was used to calculate input DNA copy numbers.

2.14. RADICA quantification of Epstein-Barr virus in serum cell-free DNA

Each 15 μL RADICA reaction consisted of 300 nM EBV-BamHIW-F3, 300 nM EBV-BamHIW-R3, 500 nM FQ reporter, 1x RPA rehydration

buffer containing 1 x RPA Pellet (TwistDx), 200 nM EnGen® Lba Cas12a (New England Biolabs), 200 nM BamHIW-3F-crRNA, 0.01 mg/mL BSA, 1x Clarity JN Solution (JN Medsys), 3 μL of serum DNA or controls, and 14 mM magnesium acetate. Each reaction mix was partitioned in the Clarity Digital PCR tube-strip (JN Medsys) followed by 42 °C incubation for 1 h in a water bath. After incubation, a Clarity™ Reader was used to read the fluorescent signal in the partitions, and Clarity™ software was used to calculate input DNA copy numbers.

3. Results

3.1. RADICA design

RADICA design schematic is illustrated in Fig. 1A. Each CRISPR-based reaction mix is sub-divided into 10,000 partitions on the chip, resulting in zero or one target molecule in each compartment with an average partition volume of 1.336 nL. The copy number of target nucleic acids is calculated based on the proportion of positive-to-negative compartments, allowing for absolute quantification of the sample (Fig. 1A). We first optimized the bulk CRISPR reaction to achieve a one-copy-per-1.336 nL partition detection sensitivity on the chip. This is equivalent to femtomolar detection sensitivity in a bulk reaction. We selected Cas12a homolog from *Lachnospiraceae bacterium* ND2006 (LbCas12a) as it showed the highest signal-to-noise ratio relative to other Cas12a homologs [21]. To test if RADICA could detect DNA with femtomolar sensitivity without pre-amplification, we incubated serially-diluted double-stranded DNA (dsDNA) with LbCas12a, CRISPR RNA (crRNA) and a FQ reporter (quenched fluorescent DNA). The detection sensitivity of the CRISPR-based method without pre-amplification in a bulk reaction was found to be 10 pM (Supplementary Fig. 1), which did not meet the femtomolar sensitivity requirement of RADICA.

To increase the detection sensitivity, we added an isothermal amplification step using RPA, whose reaction temperature (25 °C–42 °C) is compatible with that of Cas12a (25 °C–48 °C). To avoid Cas12a-mediated cleavage of the target molecule before amplification, we designed crRNA to target single-stranded DNA (ssDNA) that is generated only after the amplification of the target molecule (Fig. 1B and C) [26]; and this crRNA showed higher sensitivity than crRNA targeting double-stranded DNA (Fig. 1D). This allowed for a one-step digital RPA-CRISPR absolute quantification method that eliminates multiple operations inherent in two-step CRISPR-based detection methods such as SHERLOCK, HOLMES and DETECTR [18,19]. It is easier to design ssDNA-targeting crRNA than traditional dsDNA-targeting crRNA, because the nuclease activity of Cas12a in ssDNA is independent of the presence of a protospacer adjacent motif (PAM) [42]. We showed that Cas12a increased the signal to noise ratio of the partitions as it further amplifies the fluorescent signals in the positive partitions (Supplementary Fig. 2).

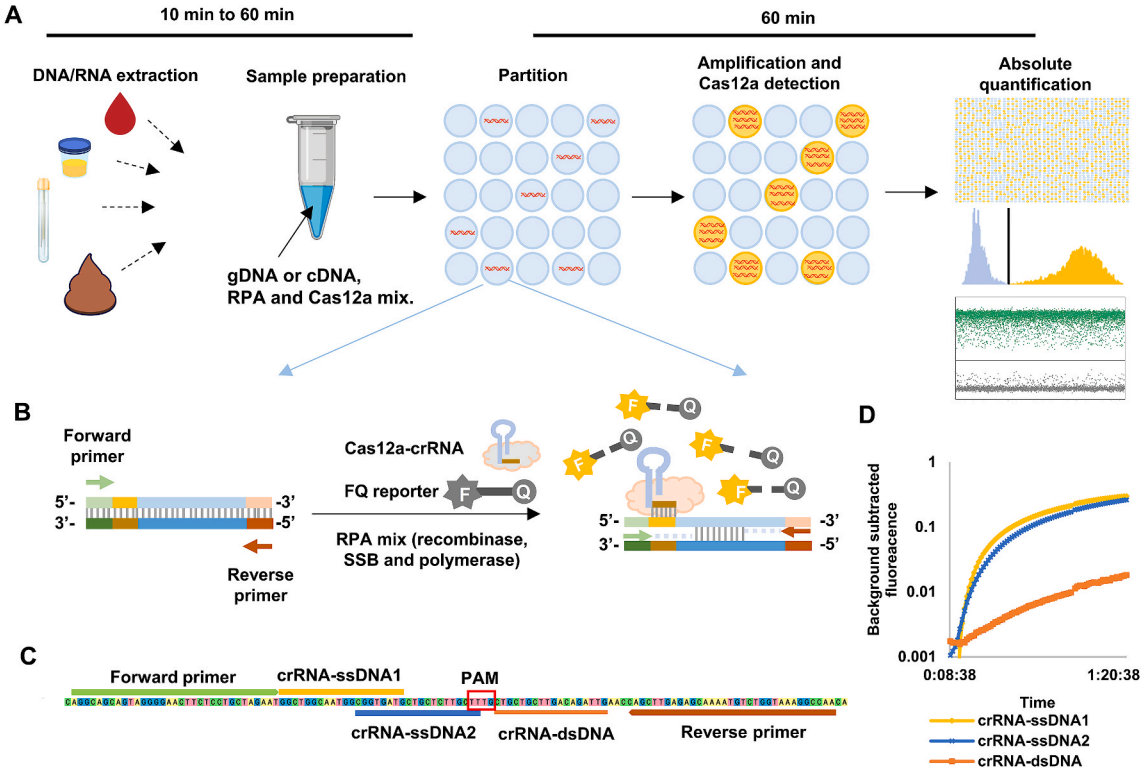

Fig. 1. Schematic illustration of RADICA. (A) RADICA workflow. Typically, after the DNA/RNA extraction step, different kinds of clinical samples can be used for the detection and quantification of various targets. The sample mixture containing DNA/cDNA, RPA reagents, and Cas12a-crRNA-FQ reporters is distributed randomly into thousands of partitions. In each partition, the DNA is amplified by RPA and detected by Cas12a-crRNA, resulting in a fluorescent signal in the partition. The proportion of positive-to-negative compartments is analyzed based on the endpoint fluorescence measurement, and the copy number of the target nucleic acids is calculated based on the Poisson distribution. (B) Illustration of RPA-Cas12a reaction in each positive partition. In each compartment containing the target molecule, RPA initiates from one DNA strand and subsequently exposes the crRNA-targeted ssDNA region on the other strand, due to the strand displacement of DNA polymerase. As the amplification proceeds, Cas12a cleaves the positive ssDNA strand, triggering its collateral cleavage activity, which in turn cleaves the proximal quenched fluorescent reporter (ssDNA-FQ reporter) to generate a fluorescence signal. At the same time, ongoing amplification of the other DNA strand exponentially amplifies the target DNA, triggering more Cas12a activation and increasing the fluorescence readout. (C) Different designs of crRNA targeting ssDNA (crRNA-ssDNA1 and crRNA-ssDNA2) or targeting dsDNA with PAM within the amplicons (crRNA-dsDNA). (D) Comparison of different designs of crRNA targeting ssDNA or dsDNA. 55 copies/μL DNA was used as a target and the RPA-Cas12a one-pot reaction was monitored at 42 °C. crRNA targeting ssDNA (ssDNA1 and ssDNA2) both showed higher sensitivity than crRNA targeting dsDNA.

3.2. RADICA optimization

Primers and crRNAs specific for dsDNA containing the SARS-CoV-2 N (nucleoprotein) gene were designed as described previously [26]. The target regions overlap those of the China CDC assay (N gene region) with some modification to meet the primer and crRNA design requirements (Supplementary Table 1). When a constant amount of dsDNA was used as a target in bulk reaction, 50 nM–250 nM Cas12a/crRNA concentration has no influence on the fluorescence intensities and reaction rates (Supplementary Fig. 3). However, fluorescence intensities of both target and negative control increased with increasing amounts of FQ reporter (from 250 nM to 10 μM) (Fig. 2A, Supplementary Fig. 4). To improve the signal to noise ratio of RADICA, we tested different FQ reporter concentrations in independent digital CRISPR reactions in the presence of target DNA, and measured the fluorescence in the dPCR fluorescence reader. In the presence of the same target DNA, proportions of the positive partitions were comparable regardless of the FQ reporter concentration used (Fig. 2B). Only background noise and positive signals generated in the reaction with 500 nM FQ reporter concentration can be clearly separated, while the reactions containing 1000 nM FQ reporter concentration yielded higher background noises, which are difficult to be separated from the positive signals (Fig. 2C). We therefore used 500 nM FQ reporter concentrations to achieve high signal-to-noise ratios for the subsequent experiments.

We combined the RPA and Cas12a reactions in a one-pot reaction. We performed the bulk reaction at 25 °C, 37 °C, and 42 °C, which fall within the reaction temperature ranges of RPA (25 °C–42 °C) and Cas12a (25 °C–48 °C). With serial dilutions of plasmid DNA, the reaction proceeded at 25 °C and 42 °C, with a limit of detection of 9.4 copies/μL (Supplementary Fig. 5). At 25 °C, the reaction was significantly slower, with lower positive signals and higher background than the reaction performed at 42 °C (Supplementary Fig. 5). We assessed the effect of different temperatures (25 °C, 37 °C, 42 °C) on reactions containing a constant amount of plasmid DNA (37.5 copies/μL). Higher temperatures accelerated the reaction (Fig. 2D). 42 °C is the optimal temperature for the RPA-Cas12a reaction.

We next investigated the earliest time that the reaction completes in all the partitions. The reaction proceeded quickly with an increase in fluorescence signals detected in some compartments at 20 min, but with a low signal-to-noise ratio at this time point (Fig. 2E). Two distinct peaks, indicating negative (left) and positive (right) partitions, were detected at 40 min with a good baseline separation (Fig. 2E). Analyzing the ratio of positive partitions on the chip at different time points revealed that the number of positive partitions reached a plateau after 40 min for all four replicates, suggesting that 40 min was the earliest time that the reactions in all the partitions have completed (Fig. 2F). To ensure all the micro-reactions are completed, all subsequent experiments were therefore performed for 60 min.

3.3. Absolute quantification of SARS-CoV-2 DNA using RADICA

We characterized the performance of RADICA in detecting and quantifying SARS-CoV-2 and compared it to that of dPCR. Linearized plasmids containing the SARS-CoV-2 N gene were serially diluted and used as the target DNA in the aforementioned optimized RADICA or dPCR reactions. A proportional increase in the number of positive partitions with increasing concentrations of the target DNA was detected by RADICA (Fig. 3A), indicating the analytical linearity of RADICA over three orders of magnitude. To test the robustness and reproducibility of RADICA, we performed at least ten independent RADICA reactions on

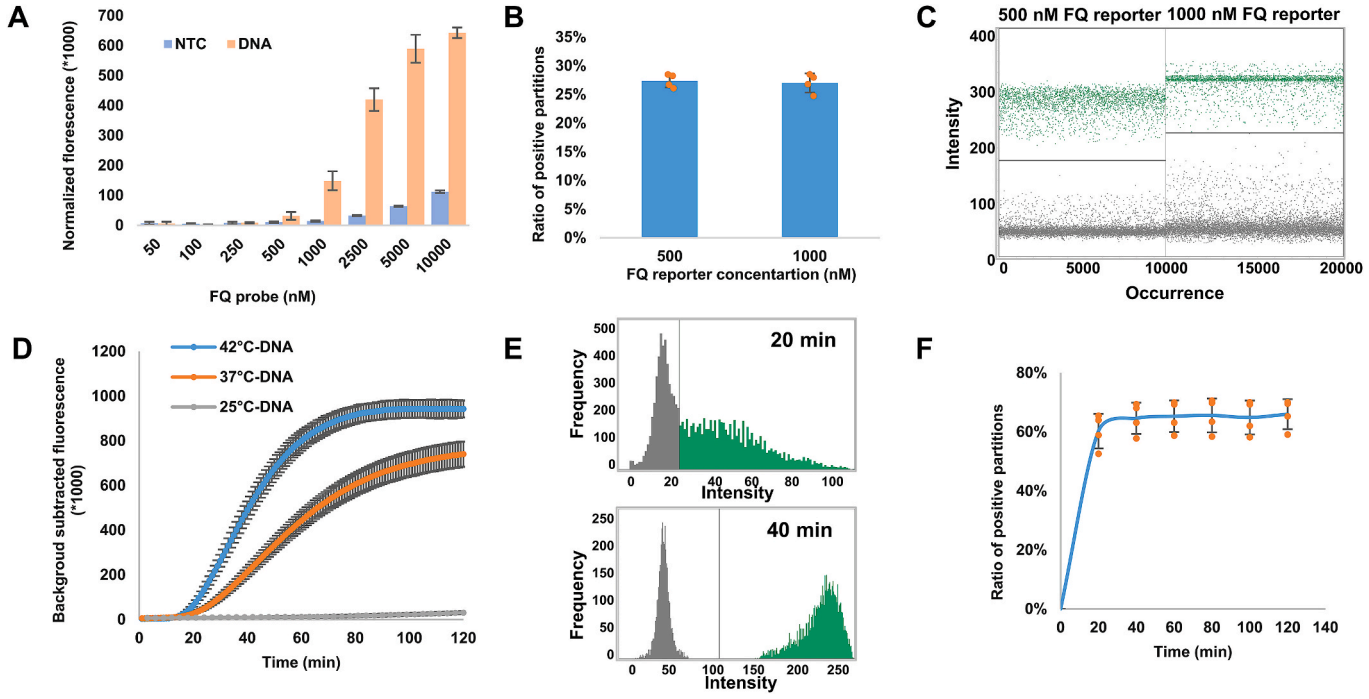

Fig. 2. Optimization of RADICA. (A) Fluorescence signal of DNA and non-template control obtained with FQ reporters at concentrations ranging from 50 nM to 10,000 nM. (B) Histogram showing ratios of positive partitions on the chip with FQ reporters, at concentrations of 500 or 1000 nM, in the presence of target DNA (4 replicates for each FQ reporter concentration). (C) Fluorescence intensity of the negative partitions (background noise, dark gray) and positive partitions (positive signals, green) on the chip obtained with FQ reporters at concentrations of 500 or 1000 nM. (D) RPA-Cas12a one-pot reaction of plasmid DNA at different temperatures (25 °C, 37 °C, and 42 °C). (E) Fluorescence intensity of the partitions on the chip at two time points. The x-axis represents fluorescence intensity while the y-axis represents the frequency of the partitions. The left peak (low fluorescence level; dark gray) on the fluorescence intensity histogram represents the negative partitions while the right peak (high fluorescence level; green) indicates the positive partitions. As the CRISPR reaction proceeds, the fluorescence levels of the positive partitions increase and the right peak shifts further to the right. (F) The proportion of positive partitions at different time points of RADICA. Starting at 40 min, the fluorescence signal plateaus and the ratio of positive partitions reach a stable level. (For interpretation of the references to colour in this figure legend, the reader is referred to the Web version of this article.)

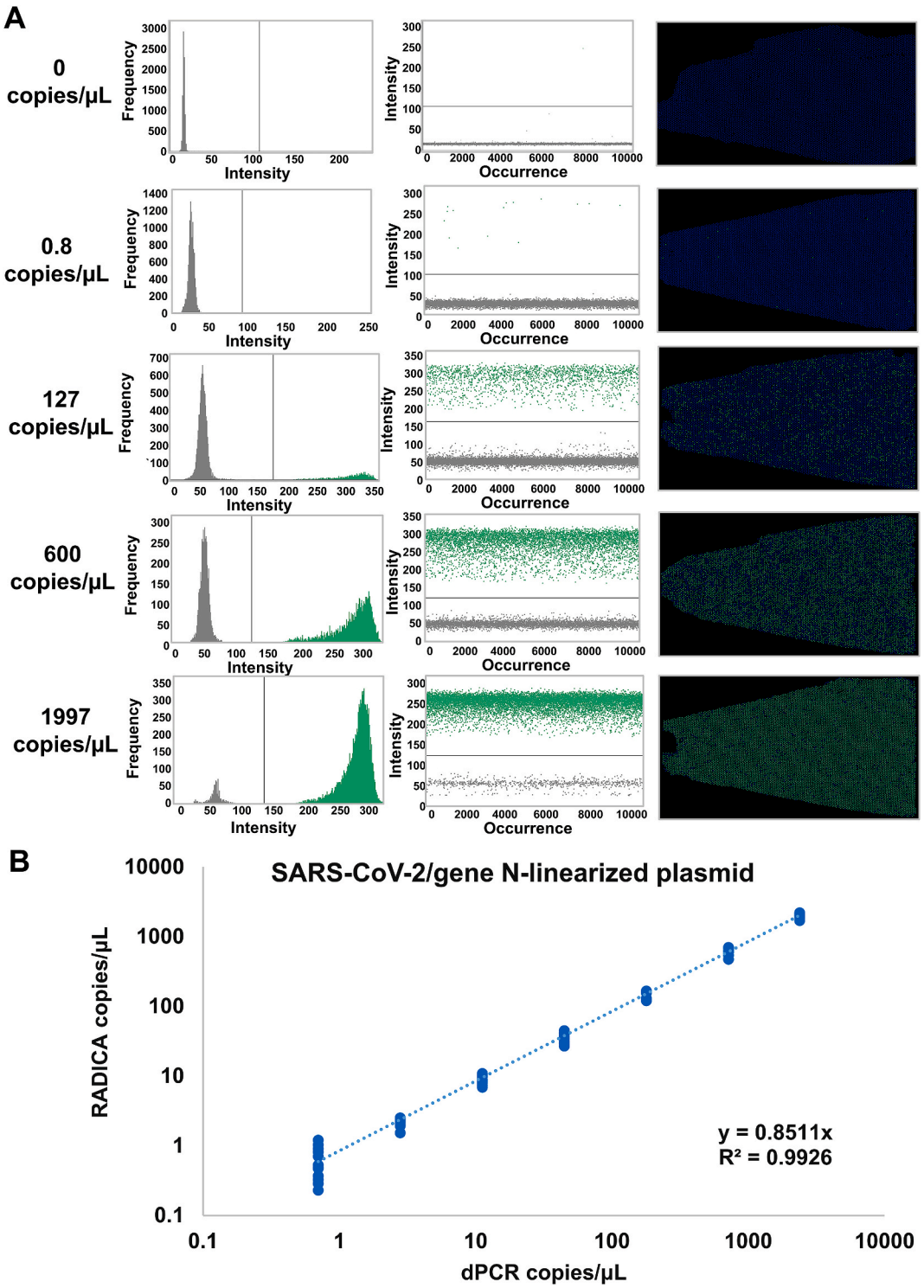

Fig. 3. RADICA-based detection of different concentrations of SARS-CoV-2 N gene DNA. (A) Fluorescence intensity histogram, scatter plot, and position plot of the partitions on the chip for serial dilutions of DNA. Four dilutions of linearized plasmid DNA encoding the SARS-CoV-2 N gene (0.8, 127, 600, 1997 copies/μL) and one non-template control (without plasmid DNA) were used as input DNA. The x-axis represents fluorescence intensity while the y-axis represents the frequency of the partitions. The left peak (low fluorescence level; dark gray) on the fluorescence intensity histogram represents the negative partitions while the right peak (high fluorescence level; green) indicates the positive partitions. In the scatter plot and position plot, each dot represents one partition on the chip. Green dots represent positive partitions with a high fluorescence level while gray or blue dots correspond to negative partitions with a low fluorescence level. (B) Comparison of the absolute quantification of RADICA and dPCR. Each point represents one sample. The original linearized plasmid DNA concentration was measured by using dPCR and diluted to different concentrations (x-axis). The diluted DNA was then measured by using the RADICA. The calculated RADICA DNA concentrations are plotted on the y-axis. (For interpretation of the references to colour in this figure legend, the reader is referred to the Web version of this article.)

different days. The inter-day coefficient of variation (CV) was ≤15% except for the lowest dilution (0.6 copies/μL), indicating the lower limit of quantification (LLoQ) of this method is 2.2 copies/μL of the viral genome (fulfils ≤15% CV criterion; Supplementary Table 2). The limit of blank (LoB) is 0.413 copies/μL, which is half of the calculated lower limit of detection (LLoD), 0.897 copies/μL (Supplementary Table 2). To assess the accuracy of nucleic acids detection for RADICA compared to dPCR, we plotted the DNA concentrations measured by RADICA against the corresponding DNA concentrations obtained by dPCR. Linear regression analysis revealed an R^2 value of above 0.99 across a dynamic range from 0.6 to 2027 copies/μL, indicating that RADICA showed strong linear correlations with dPCR (Fig. 3B). These data highlight the high sensitivity, accuracy and precision of RADICA for the absolute quantification of nucleic acids.

3.4. Accuracy analysis of RADICA-based quantification on circular plasmid

Plasmids are routinely used as reference DNA or standards; and conformational changes in supercoiled DNA can have a profound effect on PCR-based quantification [43–45]. Single-molecule amplification of non-linearized plasmids was unsuccessful in a PCR-based study, resulting in an underestimation for circular plasmid quantification in some dPCR machines [46,47]. To test whether plasmid conformation affects the accuracy of RADICA, undigested plasmids containing SARS-CoV-2 N gene were serially diluted and used for digital PCR or RADICA reactions. Concentrations of non-linearized plasmids measured by dPCR were half of those detected for linearized plasmids (Fig. 4D), indicating that the accuracy of dPCR is influenced by plasmid conformation as previously reported [46,47]. Compared to dPCR, RADICA showed a higher amplification efficiency of supercoiled plasmid DNA, as evidenced by the higher positive compartments ratio (Fig. 4A and B). RADICA concentrations of non-linearized plasmids were highly concordant with those of linearized plasmids (Fig. 4C), indicating that the accuracy of RADICA is not affected by plasmid conformation.

3.5. Specificity analysis of RADICA-based detection

Primer and crRNA designs are key in determining the specificity of CRISPR-based nucleic acids detection. RPA tolerates up to nine nucleotide base-pair mismatches across primer and probe binding sites [39]. To specifically detect SARS-CoV-2 with RADICA, primers and crRNAs would have to specifically bind the SARS-CoV-2 target DNA but not the DNA of other related coronaviruses. We analyzed the binding sites of the primers and crRNAs that were originally designed based on the consensus sequence of the genomes of 264 SARS-CoV-2 strains, available on the GISAID database [26,34,35]. These consensus sequences were aligned with the corresponding regions of SARS-CoV-2-related beta coronaviruses, such as SARS-CoV, MERS-CoV, and human coronaviruses Human-CoV 229E/HKU1/NL63/OC43. No cross-binding regions were observed with the SARS-CoV-2-related coronaviruses analyzed (Fig. 5A). Although the five base-pair mismatches between the primers of SARS-CoV-2 and those of its closest relative SARS-CoV were below the nine variation tolerance threshold for RPA, the seven base-pair mismatches in crRNA regions could increase the specificity of the assay. We assayed the bulk RPA-Cas12a reaction targeting plasmids encoding the complete N gene from SARS-CoV-2, SARS-CoV, and MERS-CoV (Fig. 5B and C). Positive fluorescence signals were observed with the SARS-CoV-2 plasmid but not the SARS-CoV or MERS-CoV plasmid (Fig. 5B and C). The absence of cross-reactivity with other related coronaviruses tested validates the specificity of RADICA for SARS-CoV-2.

3.6. Background human DNA tolerance analysis of RADICA

RPA reactions can be inhibited by high concentrations of background

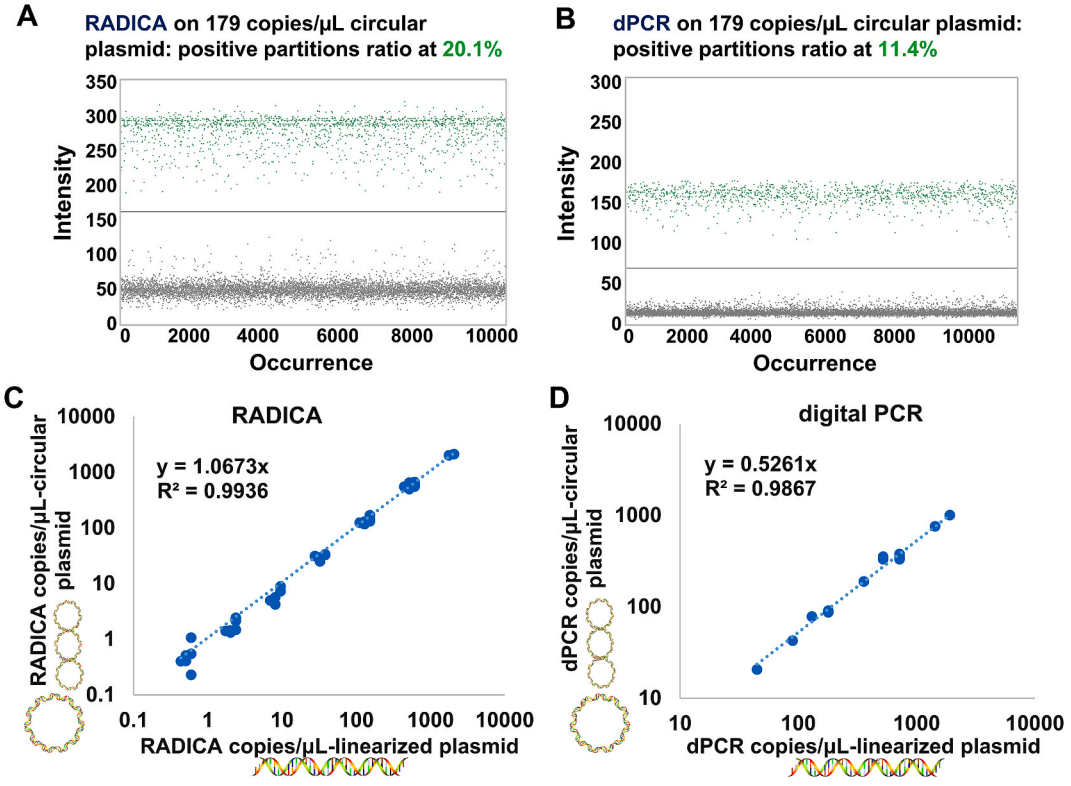

Fig. 4. The effect of plasmid conformation on the accuracy of RADICA and dPCR. (A, B) The positive and negative partitions of RADICA (A) and dPCR (B) on detection of 179 copies/μL circular plasmids. (C, D) Comparison of the absolute quantification for linearized plasmid and circular plasmid of RADICA (C) and dPCR (D).

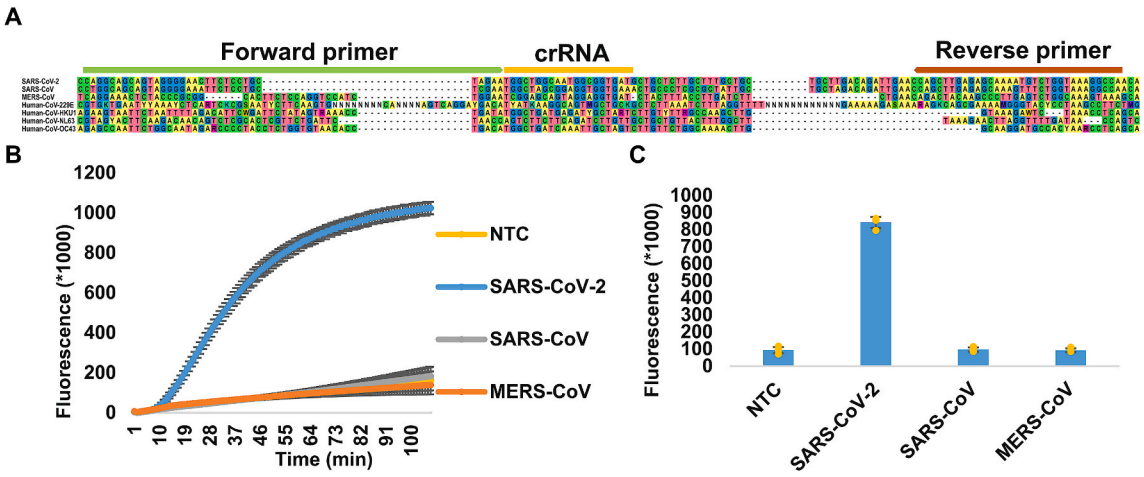

Fig. 5. Specificity analysis for SARS-CoV-2. (A) Sequence alignment of the SARS-CoV-2 target region (N gene) and the corresponding regions on other human coronaviruses. (B) Time course reaction of RPA-Cas12a assay on SARS-CoV-2, SARS-CoV, and MERS-CoV N gene DNA target. The same concentration (25,000 copies/μL) of the N gene target from different coronaviruses was tested by the bulk RPA-Cas12a assay. (C) Specificity of RPA-Cas12a assay for detection of the SARS-CoV-2 N gene.

human DNA [48,49]. We tested for possible inhibitory effects of background DNA on reactions carried out in small partitions. In an RPA-Cas12a reaction with 400 copies/μL of target DNA, 1 ng/μL of background human DNA (4350 human cells per reaction) did not affect the RADICA reaction (Supplementary Fig. 6A). We observed inhibition of the reaction containing 2 ng/μL of background human DNA, and complete inhibition of the reaction containing >5 ng/μL of background human DNA (Supplementary Fig. 6A). Since input DNA concentration used for RADICA-based detection is typically below 1 ng/μL, our findings support that background DNA does not inhibit the RADICA reaction of samples within the dynamic range to be used for testing.

The tolerance of RPA for background DNA was previously reported to depend on target DNA concentrations present in the reaction [48,49]. We tested the effect of 1 ng/μL of background human DNA on RADICA reactions with various concentrations of target DNA (Supplementary Fig. 6B). 1 ng/μL of background DNA did not affect reactions containing target DNA concentrations within the dynamic range of dPCR detection, i.e., 0.6 to 2027 copies/μL (Supplementary Fig. 6B). Our findings confirm that background human DNA in the sample does not affect the absolute quantification of nucleic acids by RADICA.

3.7. Quantitative detection of SARS-CoV-2 RNA using RADICA

As SARS-CoV-2 is an RNA virus, we tested whether RADICA could be combined with reverse transcription (RT) in a one-pot reaction for the absolute quantification of RNA. The sensitivity of the one-pot RT-RPA-Cas12a bulk reaction was lower-than-expected, with an LoD at 244 copies/μL, with an increased sensitivity (61 copies/μL) when two reverse primers were used (Fig. 6A–C). We then digitalized the one-pot RT-RPA-Cas12a reaction using digital chips and tested the results with various concentrations of RNA. Notably, we can see a good linear correlation between the target RNA concentration and the percentage of positive partitions (Fig. 6D). When Poisson distribution was used to calculate the copy number of RNA, 1 copy of input RNA resulted in an increase of only 0.0177 copies as calculated by RADICA, likely due to "molecular dropout" or low filling rate which was also observed in previous studies [29,30,50,51] (Supplementary Fig. 7). We found that using two reverse primers instead of one reverse primer could increase the positive partition ratio for the same concentration of target RNA (Fig. 6E). Using the two-reverse-primer strategy, we designed two sets of primers/crRNA targeting different regions of N gene (N0 region: 478–620 bp, N1 region: 597–754 bp, Fig. 6A) and tested the behavior of RADICA on serial dilutions of SARS-CoV-2 RNA in the background of 1 ng/μL human genomic DNA. Excellent linear relationships were observed between the RNA copy number and the positive partition ratio in both the two primers/crRNA sets (Fig. 6F and G). Using both primer/crRNA sets, 1.2 copies/μL of RNA could be detected on the digital chip, which is much sensitive than the bulk reaction (Fig. 6H and I). These results support that RADICA can quantitatively detect RNA directly with better sensitivity than bulk reactions.

3.8. Absolute quantification of Epstein-Barr virus from infected B cells by RADICA

We tested the ability of RADICA to perform absolute quantification on Epstein-Barr virus (EBV), a member of the human herpesvirus reported as viral contamination in the biologic and cell manufacturing process [1]. To design primers and crRNA that were universal to both type I and type II EBV, we analyzed the genomes of 16 EBV strains and identified the conserved regions across all 16 strains. A conserved DNA region within the Epstein-Barr nuclear antigen 1 (EBNA1) and repetitive BamHI-W sequences were used as the target sequences (Fig. 7A). Viral DNA extracted from chemically-induced EBV-harboring human B cells, diluted to concentrations ranging from 0.5 to 2100 copies/μL, was used as the target DNA in both RADICA and dPCR reactions. For RADICA-based detection, samples loaded in the partition chip were incubated for 1 h at 42 °C, followed by endpoint fluorescence detection and copy number determination. Notably, the positive partition signal increased with an increase in the concentration of input EBV DNA (Fig. 7B). The copy numbers measured by RADICA are in full concordance (R^2 value > 0.98) with those measured by dPCR (Fig. 7C and D). Our findings validate the accuracy and sensitivity of RADICA for the absolute quantification of viral DNA within an hour in human samples, a four-fold reduction in reaction time compared to dPCR-based detection.

3.9. Clinical validation of RADICA and comparison with qPCR and dPCR

To validate RADICA in clinical samples, we compared RADICA with qPCR- and dPCR-based quantification methods to analyze the EBV load in 79 serum samples obtained from 39 nasopharyngeal cancer (NPC) patients and 40 healthy controls. NPC is an EBV-associated malignancy and the circulating EBV cell-free DNA is elevated in 53–96% of NPC patients [37]. Cell-free DNA from 79 frozen serum samples were blinded and the viral load was quantified using the EBV BamHI-W target. First, to confirm the integrity of the frozen serum samples after long-term storage, qPCR-based quantification of the EBV load in each frozen

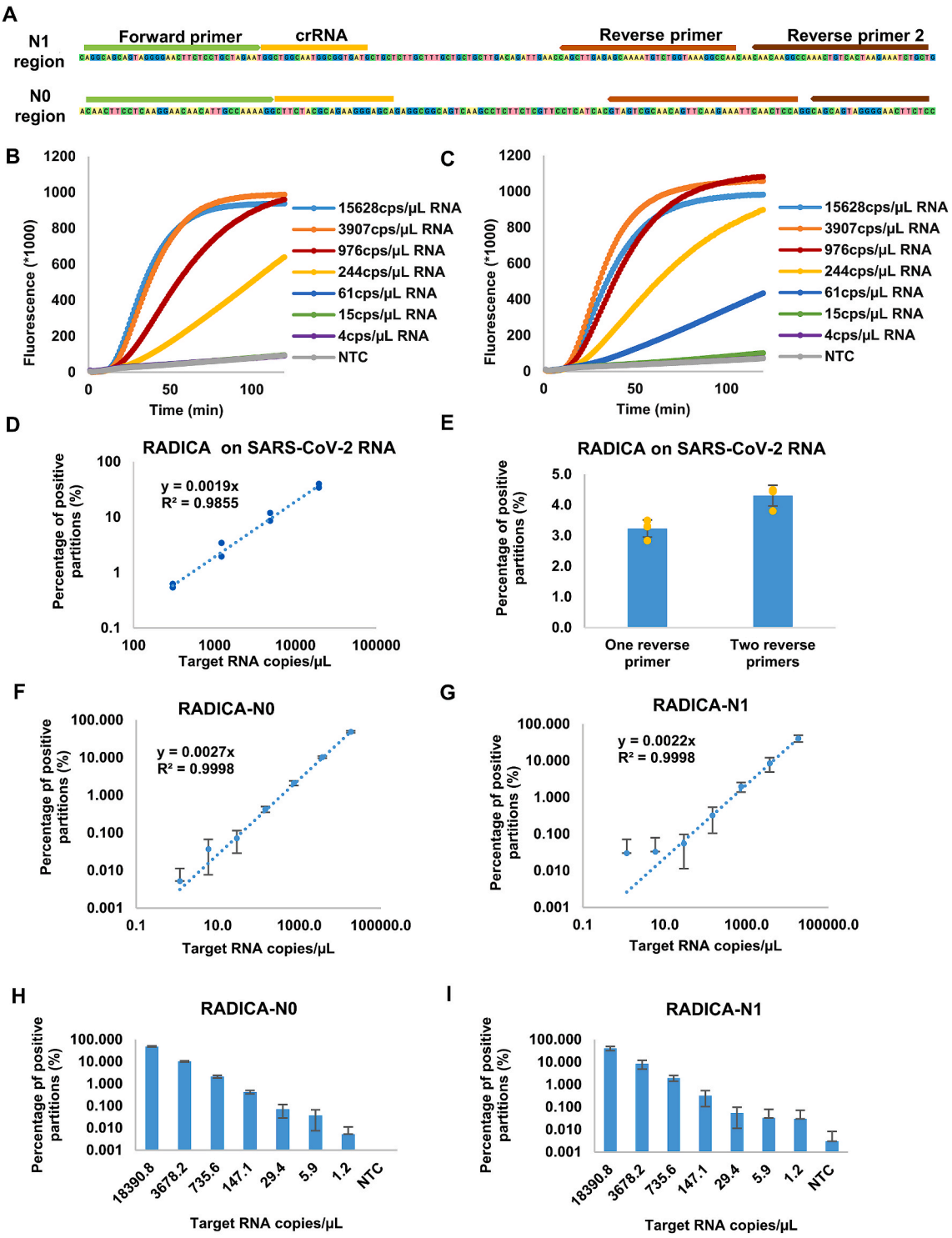

Fig. 6. RADICA reaction on RNA. (A) Design of two-reverse-primers to increase the sensitivity. One reverse primer design only includes normal forward and reverse primer and two-reverse-primers design add a reverse primer 2 in addition to normal forward and reverse primer. (B, C) Bulk RPA-Cas12a reaction on RNA at different concentrations with normal one reverse primer design (B) or two-reverse-primers design (C). (D) Correlation of positive partition percentage of RADICA and target SARS-CoV-2 RNA copy number using normal primer design. (E) Comparison of RADICA's performance on normal one reverse primer design and two-reverse-primers design. 1400 copies/μL of RNA were processed using normal one reverse primer design and two-reverse-primers design. The ratio of positive partitions increased when using two reverse primers. (F, G) Correlation of positive partition percentage of RADICA and target SARS-CoV-2 RNA copy number using two-reverse-primers' design. (H, I) Sensitivity analysis of RADICA in direct detecting SARS-CoV-2 RNA using two-reverse-primers' design.

serum sample was performed and found to be comparable with that obtained previously using the fresh serum (Supplementary Fig. 8). We next compared dPCR- and RADICA-based EBV quantification with that obtained from qPCR on the same serum samples, and found a high correlation between both methods and qPCR, with RADICA demonstrating a higher correlation with qPCR ($r = 0.872$, $p = 1.28e^{-25}$) compared to dPCR ($r = 0.831$, $p = 2.51e^{-21}$) (Fig. 8A and B). These results suggest the superior performance of RADICA over dPCR and the

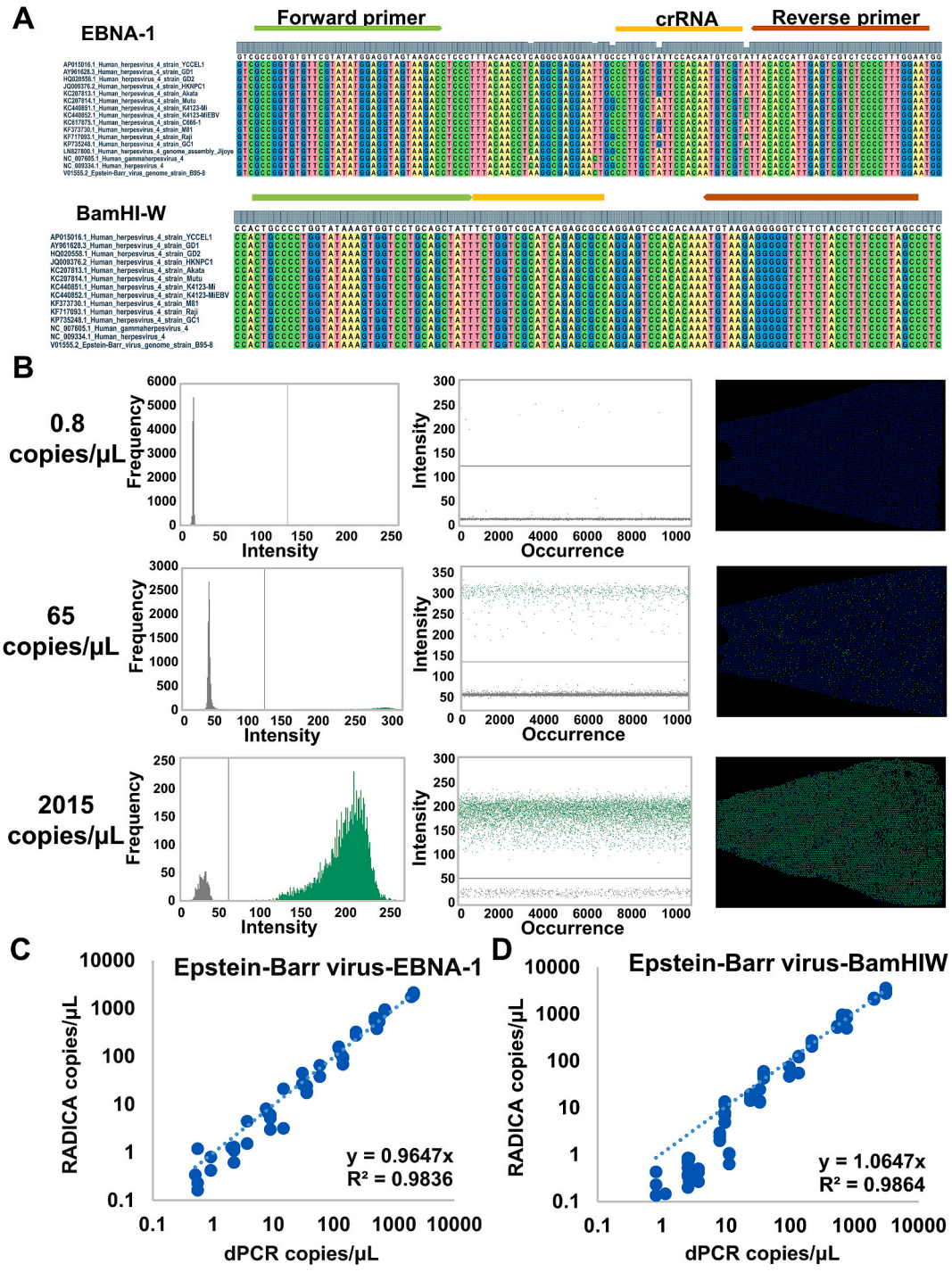

Fig. 7. Absolute quantification of Epstein-Barr virus (EBV) by RADICA. (A) Primer and crRNA design for RADICA assay specific for EBV. (B) Fluorescence intensity histogram, scatter plot, and position plot of the partitions on the chip on serially-diluted EBV DNA. (C, D) A comparison of the absolute quantification values obtained from RADICA and dPCR using various concentrations of EBV DNA.

ability of RADICA to match the clinically used qPCR-based detection of EBV in serum samples.

As EBV cell-free DNA is routinely used to monitor the virus load in NPC patients after treatment [52], frozen serum samples obtained from 22 NPC patients at their initial diagnoses, one year after treatment and the point of recurrence were blinded, and EBV loads were quantified by qPCR, dPCR and RADICA (Fig. 8C and D). Similar to qPCR and dPCR, RADICA-based EBV quantification on the 22 NPC patients showed that the viral load in the serum decreased after treatment and increased at the time of recurrence, suggesting that RADICA's ability to absolutely quantify nucleic acids can be used to monitor and compare viral load over time in NPC patients' following treatment (Fig. 8C). When analyzing the DNA copy number in each of the patients, we noted that the low EBV load in serum cell-free DNA in NPC samples (most of them ~1 copy/μL, equals to 12 copies per reaction), as well as the fact that EBV can be detected in healthy individuals further challenged the sensitivity and quantification ability of these three methods. Despite the low copy number nature of the cell-free DNA samples, RADICA is still in higher concordance with qPCR results than dPCR by detecting EBV DNA in patients 6 and 15 at initial diagnosis and patient 4 at the time of

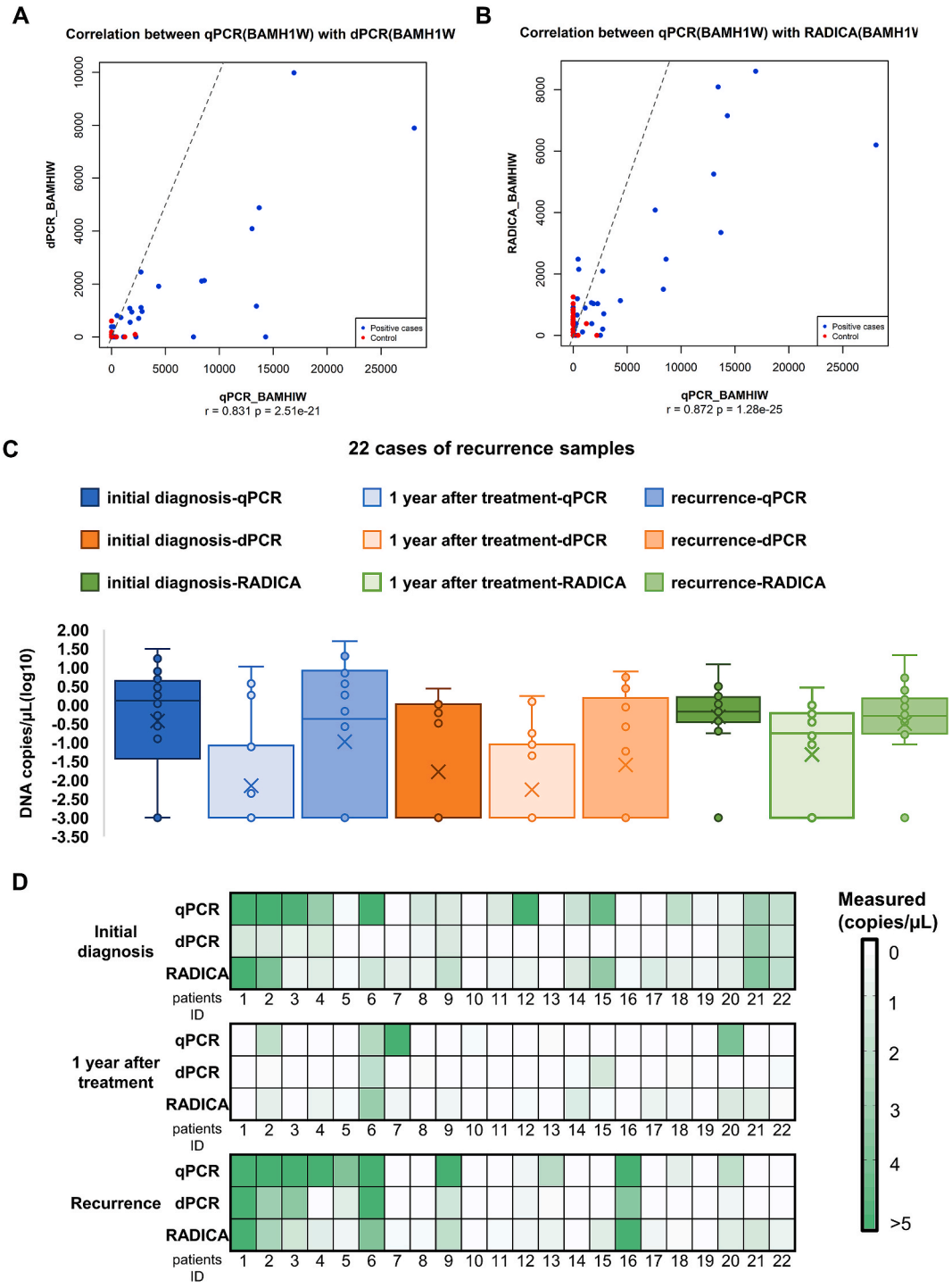

Fig. 8. Validation of RADICA on clinical samples. (A) Correlation between qPCR- and dPCR-based EBV BamHI-W target detection in 79 serum samples. (B) Correlation between qPCR- and RADICA-based EBV BamHI-W target detection in 79 serum samples. (C) Box and Whisker plot of the EBV viral load in 22 NPC patients at the point of initial diagnosis, one year after treatment, and at the point of recurrence. (D) Heat map displaying the measured EBV DNA copy number in each of the 22 NPC patients at the point of initial diagnosis, one year after treatment, and at the point of recurrence by qPCR, dPCR and RADICA.

recurrence while dPCR cannot (Fig. 8D). Together, these results demonstrate the ability of RADICA in the absolute quantification of viral load in clinical samples.

4. Discussion and conclusions

We have developed a rapid and accurate digital CRISPR method for the absolute quantification of nucleic acids. The performance characteristics of this method were validated using SARS-CoV-2 synthetic DNA/RNA and EBV DNA in clinical samples, and compared to the qPCR and dPCR methods, the current gold standard. The significant advantage of RADICA over dPCR is its speed: RADICA can perform absolute quantification rapidly within an hour, which is four times faster than current dPCR-based detection. RADICA also achieved sensitivity and detection limits (LoD 0.897 copy/μL) comparable with those of qPCR and other isothermal methods, such as SHERLOCK, HOLMES and

DETECTR, with the ability of absolute quantification (Supplementary Table 3).

The isothermal feature of RADICA-based detection assay confers faster amplification of the target nucleic acids using a simple constant-temperature heat bath, enabling rapid detection that can be deployed even in low-resource areas. In recent years, other digital isothermal methods, such as RPA- or LAMP-based digital PCR methods, have been developed for detecting a variety of nucleic acids targets [53–59]. However, these methods are limited by their low specificity, due to the inherent tolerance of RPA/LAMP-based methods for base-pair mismatches as compared to traditional PCR methods [57,58,60–65]. RADICA overcomes this by exploiting the specificity conferred by the Cas12a-crRNA-based targeting system, as recent studies showed that LbCas12a is very sensitive with mismatches between the crRNA and target region [19,21,66]. Furthermore, the collateral cleavage activity of Cas12a amplifies the signal and thus increases the signal-to-noise ratio in each individual partition.

Another advantage of RADICA over other CRISPR-based methods [20–25] is its one-pot reaction design, which reduces manual manipulation and increases reproducibility. In this streamlined one-pot reaction, both nucleic acids amplification and CRISPR-based detection are combined into a single step in a closed tube, significantly reducing the risk of cross-contamination between samples during batch processing. A major drawback of current CRISPR-based methods is the complexity of designing appropriate crRNAs that are limited to target regions in proximity to a PAM. This limitation may potentially complicate CRISPR-based virus detection since mutations in the viral PAM sequence may disable recognition by the Cas protein as the virus evolves. In contrast, our simpler digital CRISPR crRNA design is independent of the PAM sequence because it targets single-stranded DNA generated after amplification [42].

RADICA reported here uses commercially available chips and devices that can potentially be adapted to other devices in common use in hospitals and service laboratories, such as QuantStudio 3D Digital PCR System (Thermo Fisher), QIAcuity Digital PCR System (QIAGEN), and Droplet Digital PCR System (Bio-Rad). Furthermore, RADICA offers a customizable solution that is amenable to other DNA isothermal amplification platforms such as loop-mediated isothermal amplification (LAMP) [16], rolling circle amplification (RCA) [67], and strand displacement amplification (SDA) [68], as well as the use of other Cas proteins, such as Cas13a, Cas12b, Cas14 for multiplex detection [20].

Absolute quantification of viral nucleic acids could impact widely. Viral load closely parallels transmission risk and disease severity: high SARS-CoV-2 viral loads correlate with the course of infection and mortality [14,69–72]. These reports underscore the urgent need for rapid and sensitive virus detection and quantification as the basis for clinical decision-making. Such methods are also needed for mechanistic studies, transmission studies, vaccine development, and therapeutics for COVID-19. Many diagnostic methods are available for virus detection but most do not allow for rapid and precise quantification of the viral load (Supplementary Table 3). RADICA could fill this gap in the area of rapid absolute quantification.

Absolute quantification of adventitious agents can be applied in the area of gene expression analysis, rare mutation detection, liquid biopsy, gene editing detection, and sequencing library quantification [73,74], which broadly expands the applications of RADICA. The advantage of RADICA over dPCR in circular DNA quantification could also improve the extrachromosomal circular DNA quantification in cancer research [75], and determine the replication competency of adventitious agents in the manufacturing processes of biologic for cell therapy, applications in pharmaceutical, environmental, public health, security and food industry [1,4].

Credit author statement

X.W., T.K.L., and H.Y. designed the research. X.W. developed the RADICA, performed the experiment, and analyzed the data. C.K.G. performed the DNA extraction of the EBV clinical sample and the clinical sample data analysis. C.C. performed the Epstein-Barr virus culture and DNA extraction from Jijoye cells. J.K.T., K.S.L. and D.Y.W. provided the EBV clinical samples and contributed to the clinical sample data analysis. Y.H.L., S.S., T.K.L., and H.Y. provided mentorship and feedback. X. W. wrote the original draft and all authors reviewed and edited the manuscript.

Data availability

The authors declare that all data supporting the findings of this study are available within the paper (and its supplementary information files). Correspondence and requests for materials should be addressed to H.Y. and T.K.L.

Declaration of competing interest

The authors declare the following financial interests/personal relationships which may be considered as potential competing interests: X. W., T.K.L., and H.Y. are co-inventors on patent filings related to the published work. T.K.L. is a co-founder of Senti Biosciences, Synlogic, Engine Biosciences, Tango Therapeutics, Corvium, BiomX, Eligo Biosciences, Bota.Bio, Avendesora, and NE47Bio. T.K.L. also holds financial interests in nest.bio, Armata, IndieBio, MedicusTek, Quark Biosciences, Personal Genomics, Thryve, Lexent Bio, MitoLab, Vulcan, Serotiny, Avendesora, Pulmobiotics, Provectus Algae, Invaio, NSG Biolabs. H.Y. declares holding equity in Invitrocue, Osteopore, Histoindex, Vasinfuse, Ants Innovate, Synally Futuristech and Pishon Biomedical that have no conflict of interest with the work reported in this paper.

Acknowledgments

We thank Karen Pepper (MIT) and Scott A. Rice (NTU) for their careful editing and helpful comments on the manuscript. This work was supported by the National Research Foundation, Prime Minister's Office, Singapore under its Campus for Research Excellence and Technological Enterprise (CREATE) programme, through Singapore MIT Alliance for Research and Technology (SMART): Critical Analytics for Manufacturing Personalised-Medicine (CAMP) Inter-Disciplinary Research Group. The processing of clinical samples was supported by the National Medical Research Council, Singapore (Grant no: CIRG18-nov-0045).

Appendix A. Supplementary data

Supplementary data to this article can be found online at https://doi.org/10.1016/j.biomaterials.2021.120876.

References

[1] P.W. Barone, M.E. Wiebe, J.C. Leung, I.T.M. Hussein, F.J. Keumurian, J. Bouressa, et al., Viral contamination in biologic manufacture and implications for emerging therapies, Nat. Biotechnol. 38 (2020) 563–572.
[2] R.H. Sedlak, K.R. Jerome, Viral diagnostics in the era of digital polymerase chain reaction, Diagn. Microbiol. Infect. Dis. 75 (2013) 1–4.
[3] K. Katsarou, E. Bardani, P. Kallemi, K. Kalantidis, Viral detection: past, present, and future, Bioessays : News Rev. Mole. Cell. Develop. Biol. 41 (2019), e1900049.
[4] Guidance for Industry, Testing of retroviral vector-based human gene therapy products for replication competent retrovirus during product manufacture and patient follow-up, U.S. Food Drug Administ. (2020). https://www.fda.gov/media/113790/download.
[5] O. Vandenberg, D. Martiny, O. Rochas, A. van Belkum, Z. Kozlakidis, Considerations for diagnostic COVID-19 tests, Nat. Rev. Microbiol. 19 (2021) 171–183.
[6] M. Boeckh, M. Huang, J. Ferrenberg, T. Stevens-Ayers, L. Stensland, W.G. Nichols, et al., Optimization of quantitative detection of cytomegalovirus DNA in plasma by real-time PCR, J. Clin. Microbiol. 42 (2004) 1142–1148.

[7] C.M. Hindson, J.R. Chevillet, H.A. Briggs, E.N. Gallichotte, I.K. Ruf, B.J. Hindson, et al., Absolute quantification by droplet digital PCR versus analog real-time PCR, Nat. Methods 10 (2013) 1003–1005.
[8] S.J. Salipante, K.R. Jerome, Digital PCR—an emerging technology with broad applications in microbiology, Clin. Chem. 66 (2020) 117–123.
[9] R.T. Hayden, Y. Sun, L. Tang, G.W. Procop, D.R. Hillyard, B.A. Pinsky, et al., Progress in quantitative viral load testing: variability and impact of the WHO quantitative international standards, J. Clin. Microbiol. 55 (2017) 423–430.
[10] A.S. Whale, J.F. Huggett, S. Cowen, V. Speirs, J. Shaw, S. Ellison, et al., Comparison of microfluidic digital PCR and conventional quantitative PCR for measuring copy number variation, Nucleic Acids Res. 40 (2012) e82–e.
[11] J. Kim, M.A.A. Mohamed, K. Zagorovsky, W.C.W. Chan, State of diagnosing infectious pathogens using colloidal nanomaterials, Biomaterials 146 (2017) 97–114.
[12] X. Liu, J. Feng, Q. Zhang, D. Guo, L. Zhang, T. Suo, et al., Analytical comparisons of SARS-COV-2 detection by qRT-PCR and ddPCR with multiple primer/probe sets, Emerg. Microb. Infect. 9 (2020) 1175–1179.
[13] C. Alteri, V. Cento, M. Antonello, L. Colagrossi, M. Merli, N. Ughi, et al., Detection and quantification of SARS-CoV-2 by droplet digital PCR in real-time PCR negative nasopharyngeal swabs from suspected COVID-19 patients, PloS One 15 (2020), e0236311.
[14] F. Yu, L. Yan, N. Wang, S. Yang, L. Wang, Y. Tang, et al., Quantitative detection and viral load analysis of SARS-CoV-2 in infected patients, Clin. Infect. Dis. 71 (15) (2020) 793–798.
[15] Y. Liu, Z. Ning, Y. Chen, M. Guo, Y. Liu, N.K. Gali, et al., Aerodynamic analysis of SARS-CoV-2 in two Wuhan hospitals, Nature 582 (2020) 557–560.
[16] T. Notomi, H. Okayama, H. Masubuchi, T. Yonekawa, K. Watanabe, N. Amino, et al., Loop-mediated isothermal amplification of DNA, Nucleic Acids Res. 28 (2000). E63-E.
[17] O. Piepenburg, C.H. Williams, D.L. Stemple, N.A. Armes, DNA detection using recombination proteins, PLoS Biol. 4 (2006), e204.
[18] J.S. Gootenberg, O.O. Abudayyeh, J.W. Lee, P. Essletzbichler, A.J. Dy, J. Joung, et al., Nucleic acid detection with CRISPR-Cas13a/C2c2, Science 356 (2017) 438–442.
[19] J.S. Chen, E. Ma, L.B. Harrington, M. Da Costa, X. Tian, J.M. Palefsky, et al., CRISPR-Cas12a target binding unleashes indiscriminate single-stranded DNase activity, Science 360 (2018) 436–439.
[20] J.S. Gootenberg, O.O. Abudayyeh, M.J. Kellner, J. Joung, J.J. Collins, F. Zhang, Multiplexed and portable nucleic acid detection platform with Cas13, Cas12a, and Csm6, Science 360 (2018) 439–444.
[21] S.Y. Li, Q.X. Cheng, J.M. Wang, X.Y. Li, Z.L. Zhang, S. Gao, et al., CRISPR-Cas12a-assisted nucleic acid detection, Cell Discov. 4 (2018) 20.
[22] C. Myhrvold, C.A. Freije, J.S. Gootenberg, O.O. Abudayyeh, H.C. Metsky, A. F. Durbin, et al., Field-deployable viral diagnostics using CRISPR-Cas13, Science 360 (2018) 444–448.
[23] J.P. Broughton, X. Deng, G. Yu, C.L. Fasching, V. Servellita, J. Singh, et al., CRISPR–Cas12-based detection of SARS-CoV-2, Nat. Biotechnol. 38 (2020) 870–874.
[24] C.M. Ackerman, C. Myhrvold, S.G. Thakku, C.A. Freije, H.C. Metsky, D.K. Yang, et al., Massively multiplexed nucleic acid detection using Cas13, Nature 582 (2020) 277–282.
[25] T. Hou, W. Zeng, M. Yang, W. Chen, L. Ren, J. Ai, et al., Development and evaluation of a rapid CRISPR-based diagnostic for COVID-19, PLoS Pathog. 16 (2020), e1008705.
[26] X. Ding, K. Yin, Z. Li, R.V. Lalla, E. Ballesteros, M.M. Sfeir, et al., Ultrasensitive and visual detection of SARS-CoV-2 using all-in-one dual CRISPR-Cas12a assay, Nat. Commun. 11 (2020) 4711.
[27] L. Li, S. Li, N. Wu, J. Wu, G. Wang, G. Zhao, et al., HOLMESv2: a CRISPR-cas12b-assisted platform for nucleic acid detection and DNA methylation quantitation, ACS Synth. Biol. 8 (2019) 2228–2237.
[28] Y. Li, S. Li, J. Wang, G. Liu, CRISPR/Cas systems towards next-generation biosensing, Trends Biotechnol. 37 (2019) 730–743.
[29] J.S. Park, K. Hsieh, L. Chen, A. Kaushik, A.Y. Trick, T.H. Wang, Digital CRISPR/Cas-Assisted assay for rapid and sensitive detection of SARS-CoV-2, Adv. Sci. (2020), 2003564.
[30] X. Ding, K. Yin, Z. Li, M.M. Sfeir, C. Liu, Sensitive quantitative detection of SARS-CoV-2 in clinical samples using digital warm-start CRISPR assay, medRxiv (2020) 2020, 11.21.20236109.
[31] T. Tian, B. Shu, Y. Jiang, M. Ye, L. Liu, Z. Guo, et al., An ultralocalized Cas13a assay enables universal and nucleic acid amplification-free single-molecule RNA diagnostics, ACS Nano 15 (2021) 1167–1178.
[32] M.J. Kellner, J.G. Koob, J.S. Gootenberg, O.O. Abudayyeh, F. Zhang, SHERLOCK: nucleic acid detection with CRISPR nucleases, Nat. Protoc. 14 (2019) 2986–3012.
[33] C. Lucia, P.-B. Federico, G.C. Alejandra, An ultrasensitive, rapid, and portable coronavirus SARS-CoV-2 sequence detection method based on CRISPR-Cas12, bioRxiv (2020), 2020.02.29.971127.
[34] S. Elbe, G. Buckland-Merrett, Data, disease and diplomacy: GISAID's innovative contribution to global health, Global Challeng. 1 (2017) 33–46.
[35] Y. Shu, J. McCauley, GISAID: global initiative on sharing all influenza data – from vision to reality, Euro Surveill. 22 (2017) 30494.
[36] J.H. Vo, W.L. Nei, M. Hu, W.M. Phyo, F. Wang, K.W. Fong, et al., Comparison of circulating tumour cells and circulating cell-free epstein-barr virus DNA in patients with nasopharyngeal carcinoma undergoing radiotherapy, Sci. Rep. 6 (2016) 13.
[37] J.K. Tay, C.H. Siow, H.L. Goh, C.M. Lim, P.P. Hsu, S.H. Chan, et al., A comparison of EBV serology and serum cell-free DNA as screening tools for nasopharyngeal cancer: results of the Singapore NPC screening cohort, Int. J. Canc. 146 (2020) 2923–2931.
[38] H. Low, S.-J. Chan, G.-H. Soo, B. Ling, E.-L. Tan, Clarity™ digital PCR system: a novel platform for absolute quantification of nucleic acids, Anal. Bioanal. Chem. 409 (2017) 1869–1875.
[39] J. Li, J. Macdonald, F. von Stetten, Review: a comprehensive summary of a decade development of the recombinase polymerase amplification, Analyst 144 (2018) 31–67.
[40] D.A. Armbruster, T. Pry, Limit of blank, limit of detection and limit of quantitation, Clin. Biochem. Rev. 29 (Suppl 1) (2008) S49–S52.
[41] J.K. Tay, S.H. Chan, C.M. Lim, C.H. Siow, H.L. Goh, K.S. Loh, The role of epstein-barr virus DNA load and serology as screening tools for nasopharyngeal carcinoma. Otolaryngology–head and neck surgery, Off. J. Am. Acad. Otolaryngol. Head Neck Surg. 155 (2016) 274–280.
[42] S.Y. Li, Q.X. Cheng, J.K. Liu, X.Q. Nie, G.P. Zhao, J. Wang, CRISPR-Cas12a has both cis- and trans-cleavage activities on single-stranded DNA, Cell Res. 28 (2018) 491–493.
[43] J. Chen, F.F. Kadlubar, J.Z. Chen, DNA supercoiling suppresses real-time PCR: a new approach to the quantification of mitochondrial DNA damage and repair, Nucleic Acids Res. 35 (2007) 1377–1388.
[44] Y. Hou, H. Zhang, L. Miranda, S. Lin, Serious overestimation in quantitative PCR by circular (supercoiled) plasmid standard: microalgal pcna as the model gene, PloS One 5 (2010) e9545.
[45] M. Beinhauerova, V. Babak, B. Bertasi, M.B. Boniotti, P. Kralik, Utilization of digital PCR in quantity verification of plasmid standards used in quantitative PCR, Front. Mole. Biosci. 7 (2020).
[46] L. Dong, Y. Meng, J. Wang, Y. Liu, Evaluation of droplet digital PCR for characterizing plasmid reference material used for quantifying ammonia oxidizers and denitrifiers, Anal. Bioanal. Chem. 406 (2014) 1701–1712.
[47] L. Dong, Y. Meng, Z. Sui, J. Wang, L. Wu, B. Fu, Comparison of four digital PCR platforms for accurate quantification of DNA copy number of a certified plasmid DNA reference material, Sci. Rep. 5 (2015) 13174.
[48] E. Clancy, O. Higgins, M.S. Forrest, T.W. Boo, M. Cormican, T. Barry, et al., Development of a rapid recombinase polymerase amplification assay for the detection of Streptococcus pneumoniae in whole blood, BMC Infect. Dis. 15 (2015) 481.
[49] B. Rohrman, R. Richards-Kortum, Inhibition of recombinase polymerase amplification by background DNA: a lateral flow-based method for enriching target DNA, Anal. Chem. 87 (2015) 1963–1967.
[50] G. Nixon, J.A. Garson, P. Grant, E. Nastouli, C.A. Foy, J.F. Huggett, Comparative study of sensitivity, linearity, and resistance to inhibition of digital and nondigital polymerase chain reaction and loop mediated isothermal amplification assays for quantification of human cytomegalovirus, Anal. Chem. 86 (2014) 4387–4394.
[51] A.S. Whale, S. Cowen, C.A. Foy, J.F. Huggett, Methods for applying accurate digital PCR analysis on low copy DNA samples, PloS One 8 (2013), e58177.
[52] W.-F. Li, Y. Zhang, X.-B. Huang, X.-J. Du, L.-L. Tang, L. Chen, et al., Prognostic value of plasma Epstein–Barr virus DNA level during posttreatment follow-up in the patients with nasopharyngeal carcinoma having undergone intensity-modulated radiotherapy, Chin. J. Canc. 36 (2017) 87.
[53] F. Hu, J. Li, Z. Zhang, M. Li, S. Zhao, Z. Li, et al., Smartphone-based droplet digital LAMP device with rapid nucleic acid isolation for highly sensitive point-of-care detection, Anal. Chem. 92 (2020) 2258–2265.
[54] X. Lin, X. Huang, K. Urmann, X. Xie, M.R. Hoffmann, Digital loop-mediated isothermal amplification on a commercial membrane, ACS Sens. 4 (2019) 242–249.
[55] Y.D. Ma, W.H. Chang, K. Luo, C.H. Wang, S.Y. Liu, W.H. Yen, et al., Digital quantification of DNA via isothermal amplification on a self-driven microfluidic chip featuring hydrophilic film-coated polydimethylsiloxane, Biosens. Bioelectron. 99 (2018) 547–554.
[56] E.C. Yeh, C.C. Fu, L. Hu, R. Thakur, J. Feng, L.P. Lee, Self-powered integrated microfluidic point-of-care low-cost enabling (SIMPLE) chip, Sci. Adv. 3 (2017), e1501645.
[57] F. Shen, E.K. Davydova, W. Du, J.E. Kreutz, O. Piepenburg, R.F. Ismagilov, Digital isothermal quantification of nucleic acids via simultaneous chemical initiation of recombinase polymerase amplification reactions on SlipChip, Anal. Chem. 83 (2011) 3533–3540.
[58] F. Schuler, F. Schwemmer, M. Trotter, S. Wadle, R. Zengerle, F. von Stetten, et al., Centrifugal step emulsification applied for absolute quantification of nucleic acids by digital droplet RPA, Lab Chip 15 (2015) 2759–2766.
[59] Z. Li, Y. Liu, Q. Wei, Y. Liu, W. Liu, X. Zhang, et al., Picoliter well Array chip-based digital recombinase polymerase amplification for absolute quantification of, Nucleic Acids. PloS one. 11 (2016), e0153359.
[60] Y. Zhao, F. Chen, Q. Li, L. Wang, C. Fan, Isothermal amplification of nucleic acids, Chem. Rev. 115 (2015) 12491–12545.
[61] I.M. Lobato, C.K. O'Sullivan, Recombinase polymerase amplification: basics, applications and recent advances, Trac. Trends Anal. Chem. 98 (2018) 19–35.
[62] D. Mondal, P. Ghosh, M.A.A. Khan, F. Hossain, S. Böhlken-Fascher, G. Matlashewski, et al., Mobile suitcase laboratory for rapid detection of Leishmania donovani using recombinase polymerase amplification assay, Parasites Vectors 9 (2016) 281.
[63] R.K. Daher, G. Stewart, M. Boissinot, D.K. Boudreau, M.G. Bergeron, Influence of sequence mismatches on the specificity of recombinase polymerase amplification technology, Mol. Cell. Probes 29 (2015) 116–121.
[64] J.C. Rolando, E. Jue, N.G. Schoepp, R.F. Ismagilov, Real-time, digital LAMP with commercial microfluidic chips reveals the interplay of efficiency, speed, and

background amplification as a function of reaction temperature and time, Anal. Chem. 91 (2019) 1034–1042.
[65] P. Hardinge, J.A.H. Murray, Reduced false positives and improved reporting of loop-mediated isothermal amplification using quenched fluorescent primers, Sci. Rep. 9 (2019) 7400.
[66] K.H. Ooi, M.M. Liu, J.W.D. Tay, S.Y. Teo, P. Kaewsapsak, S. Jin, et al., An engineered CRISPR-Cas12a variant and DNA-RNA hybrid guides enable robust and rapid COVID-19 testing, Nat. Commun. 12 (2021) 1739.
[67] P.M. Lizardi, X. Huang, Z. Zhu, P. Bray-Ward, D.C. Thomas, D.C. Ward, Mutation detection and single-molecule counting using isothermal rolling-circle amplification, Nat. Genet. 19 (1998) 225–232.
[68] G.T. Walker, M.S. Fraiser, J.L. Schram, M.C. Little, J.G. Nadeau, D.P. Malinowski, Strand displacement amplification–an isothermal, in vitro DNA amplification technique, Nucleic Acids Res. 20 (1992) 1691–1696.
[69] E. Pujadas, F. Chaudhry, R. McBride, F. Richter, S. Zhao, A. Wajnberg, et al., SARS-CoV-2 viral load predicts COVID-19 mortality, Lancet Respir. Med. 8 (9) (2020), e70.
[70] S. Zheng, J. Fan, F. Yu, B. Feng, B. Lou, Q. Zou, et al., Viral load dynamics and disease severity in patients infected with SARS-CoV-2 in Zhejiang province, China, January-March 2020: retrospective cohort study, BMJ 369 (2020) m1443-m.
[71] L. Zou, F. Ruan, M. Huang, L. Liang, H. Huang, Z. Hong, et al., SARS-CoV-2 viral load in upper respiratory specimens of infected patients, N. Engl. J. Med. 382 (2020) 1177–1179.
[72] R. Wölfel, V.M. Corman, W. Guggemos, M. Seilmaier, S. Zange, M.A. Müller, et al., Virological assessment of hospitalized patients with COVID-2019, Nature 581 (2020) 465–469.
[73] M. Baker, Digital PCR hits its stride, Nat. Methods 9 (2012) 541–544.
[74] K.H. Neoh, A.A. Hassan, A. Chen, Y. Sun, P. Liu, K.-F. Xu, et al., Rethinking liquid biopsy: microfluidic assays for mobile tumor cells in human body fluids, Biomaterials 150 (2018) 112–124.
[75] H. Kim, N.-P. Nguyen, K. Turner, S. Wu, A.D. Gujar, J. Luebeck, et al., Extrachromosomal DNA is associated with oncogene amplification and poor outcome across multiple cancers, Nat. Genet. 52 (2020) 891–897.